

Photoacoustic/ultrasonic dual-mode imaging for monitoring angiogenesis and synovial erosion in rheumatoid arthritis

Zhen Wang ^{a,b,1}, Zhuangzhuang Tong ^{c,1}, Hongjiang Chen ^{a,b}, Guangshuai Nie ^{a,b}, Jia Hu ^{a,b}, Weiyang Liu ^{a,b}, Erqi Wang ^c, Bo Yuan ^c, Zhiyang Wang ^{c,*}, Jun Hu ^{a,b,**}

^a Department of Orthopaedics, The First Affiliated Hospital of Shantou University Medical College, Shantou, PR China

^b Orthopaedic Medical Research Center, The First Affiliated Hospital of Shantou University Medical College, Shantou, PR China

^c MOE Key Laboratory of Laser Life Science & Guangdong Provincial Key Laboratory of Laser Life Science, College of Biophotonics, South China Normal University, Guangzhou, PR China

ARTICLE INFO

Keywords:

Photoacoustic imaging
Ultrasonic imaging
Rheumatoid arthritis
Angiogenesis

ABSTRACT

Rheumatoid arthritis (RA) is a chronic autoimmune disease characterized by the formation of new vessels, synovial proliferation and destruction of articular cartilage. However, characteristic early diagnostic and therapeutic monitoring methods are still lacking. We report a study using a photoacoustic/ultrasound (PA/US) dual-mode imaging for RA disease. By establishing a collagen-induced (CIA) RA mouse model to classify disease states based on a subjective grading system, PA/US imaging allows real-time assessment of synovial erosion and vascular opacification within the knee joint in different disease states at high spatial resolution. The system also quantitatively monitors subcutaneous vascular physiology and morphology in the hind paw of mice, measuring the area and photoacoustic signal intensity of vascular proliferation and showing a positive correlation with disease grading. Compared to traditional subjective scoring of arthritis severity, the PA/US imaging is more sensitive i.e., vascular signals and synovial erosion can be observed early in the course of arthritis.

1. Introduction

Rheumatoid arthritis (RA) is a chronic autoimmune disease with an unclear etiology. Pathological alterations include angiogenesis of microvessels, pannus development, and degradation of cartilage and bone [1,2]. Early identification and therapeutic care are crucial since RA causes progressive joint deterioration and systemic responses, and even early death [3–6]. In general, the synovium is a membranous structure attached to the edges of the joint surface and the periphery of the articular cartilage, lines the joint capsule, and is mainly arranged over the joints, bursae and tendon sheaths. The synovial membrane is responsible for the production of synovial fluid, which acts as a lubricant and nourisher for the joints. The synovium is affected by several diseases, such as inflammatory, traumatic, degenerative and infectious diseases. In RA, synovial tissue is first affected, leading to inflammatory changes and synovial thickening, presenting with the production of vascular opacities, a characteristic pathological change in rheumatoid arthritis [7,8]. Persistent active synovitis can induce subsequent

anatomical damage, including cartilage damage, ligamentous rupture, and bone erosion. Among these, cartilage damage is strongly associated with loss of joint function and disability [5]. Clinically, X-ray and computed tomography (CT) scans are common diagnostic tools for RA [9,10], but they can only be used when the bone has deteriorated [11,12], and also lack specificity for soft tissue and blood vessels [13]. Moreover, X-ray and CT involve radiation, which may increase the risk of cancer or teratogenesis [14]. Magnetic resonance imaging (MRI) offers greater sensitivity for the identification of soft tissue and bone deterioration, and for imaging modalities of synovial lesions. MRI is more diagnostic than other methods and helps to narrow the differential diagnosis [15,16]. But it is hampered by high cost, low temporal resolution, and a narrow patient enclosure that can lead to claustrophobia [17,18]. There is an unmet need for higher sensitive, specific and non-invasive diagnostic monitoring methods to identify synovial erosions and vascular opacities at an early stage.

Photoacoustic imaging (PAI) is a new hybrid imaging method [19–22]. When a laser irradiates the imaging target, the target absorbs

* Corresponding author.

** Correspondence to: Department of Orthopaedics, First Affiliated Hospital of Shantou University Medical College, Shantou, PR China.

E-mail addresses: wzy_0617@163.com (Z. Wang), hjzkmst@126.com (J. Hu).

¹ Both authors contributed equally to this work.

<https://doi.org/10.1016/j.pacs.2023.100458>

Received 24 November 2022; Received in revised form 3 February 2023; Accepted 5 February 2023

Available online 6 February 2023

2213-5979/© 2023 The Authors. Published by Elsevier GmbH. This is an open access article under the CC BY-NC-ND license (<http://creativecommons.org/licenses/by-nc-nd/4.0/>).

photons to generate transient thermoelastic expansion that outwardly emits ultrasonic waves. The ultrasonic signal is received by an ultrasonic transducer and reconstructed by an algorithm into a three-dimensional image where the intensity of the target signal is proportional to the amount of light absorption [23]. PAI combines the advantages of optical imaging and ultrasonic imaging [24], with high spatial resolution (0.1–100 μm) [25], and deep penetration depth [26]. Endogenous luminous groups (hemoglobin, melanin, etc.) and exogenous molecules (metal nanoparticles, organic small molecules, etc.) may be excited by laser and produce a PA effect [27]. PAI can directly visualize vascular morphology with high resolution and high contrast, based on the high absorption of hemoglobin in the blood vessels. Based on these characteristics, PAI can successfully acquire the vascular morphology inside the joint [28]. Due to its non-invasive, and high contrast, real-time continuous imaging characteristics, PAI is suitable for specific and sensitive monitoring of RA. Currently, photoacoustic imaging for arthritis in mouse models mostly requires exogenous contrast agents, including Evans blue, indocyanine green, and gold nanoparticles, etc [18,29,30]. Contrast agents can enhance the signal-to-noise ratio and signal strength of photoacoustic signals, making it easier to visualize anatomical structures. However, the presence of contrast agents may be toxic and allergic and invasive, so imaging without contrast agents is more acceptable to the public. In addition, the inflammatory changes in the foot are also an important part in the mouse model of rheumatoid arthritis, but we have not retrieved any article on quantitative analysis of the foot vascular photoacoustic imaging (vessel diameter, photoacoustic signal intensity) in mice with rheumatoid arthritis, and our work is well suited to fill this gap.

As a mature imaging technology, ultrasonic imaging (USI) has been used in the diagnosis, treatment and monitor of RA. In particular, high-resolution musculoskeletal ultrasound is used to evaluate inflammation (exudation, proliferation) and structural damage (cartilage, subchondral, meniscus, bone, joint space) [31–35]. Studies have shown that musculoskeletal ultrasound can be used to monitor the disease activity of RA [35,36]. At the same time, various clinical studies have shown that USI can be used to further predict joint injury, even in the case of clinical remission of RA. Some studies have found that, through local irradiation, ultrasound can form bubbles that burst at high temperature and kill inflammatory cells, thereby reducing synovial hyperplasia and tissue damage, which may alleviate the clinical symptoms of RA patients, such as reducing morning stiffness and increasing grip strength, therefore benefits in relieving the disease and slowing its progression [37,38]. As a mature imaging technology, ultrasound and other imaging technologies can complement each other's deficiencies, such as artifacts, examination methods, and lack of clarity and resolution.

Photoacoustic and ultrasonic imaging (PA/US) systems are highly similar and can share the same ultrasonic transducer to receive signals [39]. Photoacoustic imaging provides the morphology of blood vessels within tissues, and ultrasound imaging reveals tissue structure. The dual-mode imaging of PA/US can effectively avoid artifacts and carry out high-resolution and high-contrast imaging of rheumatoid arthritis [40–42]. In small animals, previous results have shown that the intensity of PA signal images in arthritic ankles is significantly enhanced compared to normal joints, demonstrating the feasibility of PAI measurements of angiogenesis [43–45]. In addition, recent studies have addressed the use of exogenous PA contrast agents combined with drugs as the imaging or therapeutic medium for RA [29,46,47]. Currently, PAI is not only limited to animal models, and relevant imaging devices and techniques are already available in the clinic [48–50]. One study examined seven small joints in humans using a PA/US imaging system to measure relative oxygen saturation values in inflamed joints and showed that the sub-PA score was highly positively correlated with the standard clinical score for RA. There is no doubt that PAI technology has shown great application value in RA.

Using an RA mouse model, we performed PA/US dual-mode imaging without exogenous contrast agent on the knee joint and studied the

feasibility of PA/US dual-mode imaging in the diagnosis of RA. PAI was used to monitor the pannus of the knee joint, and USI was used to monitor the synovial erosion (cartilage and joint space) of the mouse joint. We hope to establish a more intuitive and effective method to diagnose early RA, so as to better guide treatment and assist future clinical translation and application.

2. Materials and methods

2.1. Collagen-induced arthritis (CIA) model

All animal experiments were approved by the Animal Ethics Committee of Shantou University Medical College. Animal experiments and experimental procedures were performed in strict accordance with institutional and national regulations. The collagen-induced arthritis (CIA) model is the most commonly used animal model for studying RA [51], adult DBA/1 mice are a susceptible model of RA. Three mice are used for each grade (0–4). We purchased a total of three batches of DBA/1 mice, 30 mice from each of the first two batches for pre-experiments and 50 mice from the third batch for formal experiments. Male DBA/1 mice (8 weeks old) were purchased from Gempharmatech Co., Ltd, and housed at 4–5 mice per cage. The light cycle was controlled at 12 h in a room at a temperature of 21 °C and 45 % humidity, and water and food were ingested ad libitum. After one week of adaptive feeding, RA mice were established in genetically susceptible mice by immunization with emulsified type II collagen in complete Freund's adjuvant (CFA). The general procedure was to add an equal amount of type II collagen (4 mg/ml) drop by drop to complete Freund's adjuvant (CFA) (4 mg/ml), which was completely mixed and emulsified in a tissue homogenizer. It is important to ensure that the procedure is performed at low temperature. Mice anesthetized with 2.5 % isoflurane were slowly injected intradermally (i.d.) with 50 μL of emulsion at a distance of 1.5 cm from the tail root. The same concentration of emulsion was re-injected in the tail 14 days after the first immunization to enhance immunity and ensure a high incidence of CIA. Based on the subjective scoring system reported in the literature [52], the mice were evaluated 21 days after injection of the modeling drug, and different disease scores were given to the onset mice for the experiments based on the degree and extent of hind paw swelling. In this process, we ensured that there were at least three mice with a similar disease score for each disease score class (0–4). In dual-modal PA/US imaging, three mice in each grade (0–4) were scanned 3 times to ensure the reliability and reproducibility of the imaging data. Before the experiment, mice were anesthetized with 3 % isoflurane and kept at rest, and the knee imaging area of the mice to be imaged was removed with commercial hair removal cream. During the experiment, the mice were secured in a special immobilization holder (used 3D printing technology to specially make a groove for mice to lie in.) on a heating pad to ensure proper imaging body position (to ensure that the imaging positions of different groups of mice were similar as far as possible) and to maintain their body temperature, and the hind limbs were secured and bent approximately 60 degrees to expose the imaging area as much as possible during the experiment. Ultrasound gel and deionized water were used to couple the PA signal between the mouse skin and the transducer. Mice with normal and different RA scores were imaged at least three times in each group. Except for the mice that died during the experiment, the remaining mice with different disease scores were imaged. The schematic diagram of the RA model and the imaging principle are shown in Fig. 1(A). In this study, PAI is used to detect angiogenesis in joints, and USI is used to assess synovial erosion.

2.2. Clinical scores and histopathological scores

2.2.1. Arthritis severity subjective assessment scoring system

Visual identification of arthritic limbs was not difficult, and the degree of swelling, erythema, and limb stiffness of the limbs (toes and

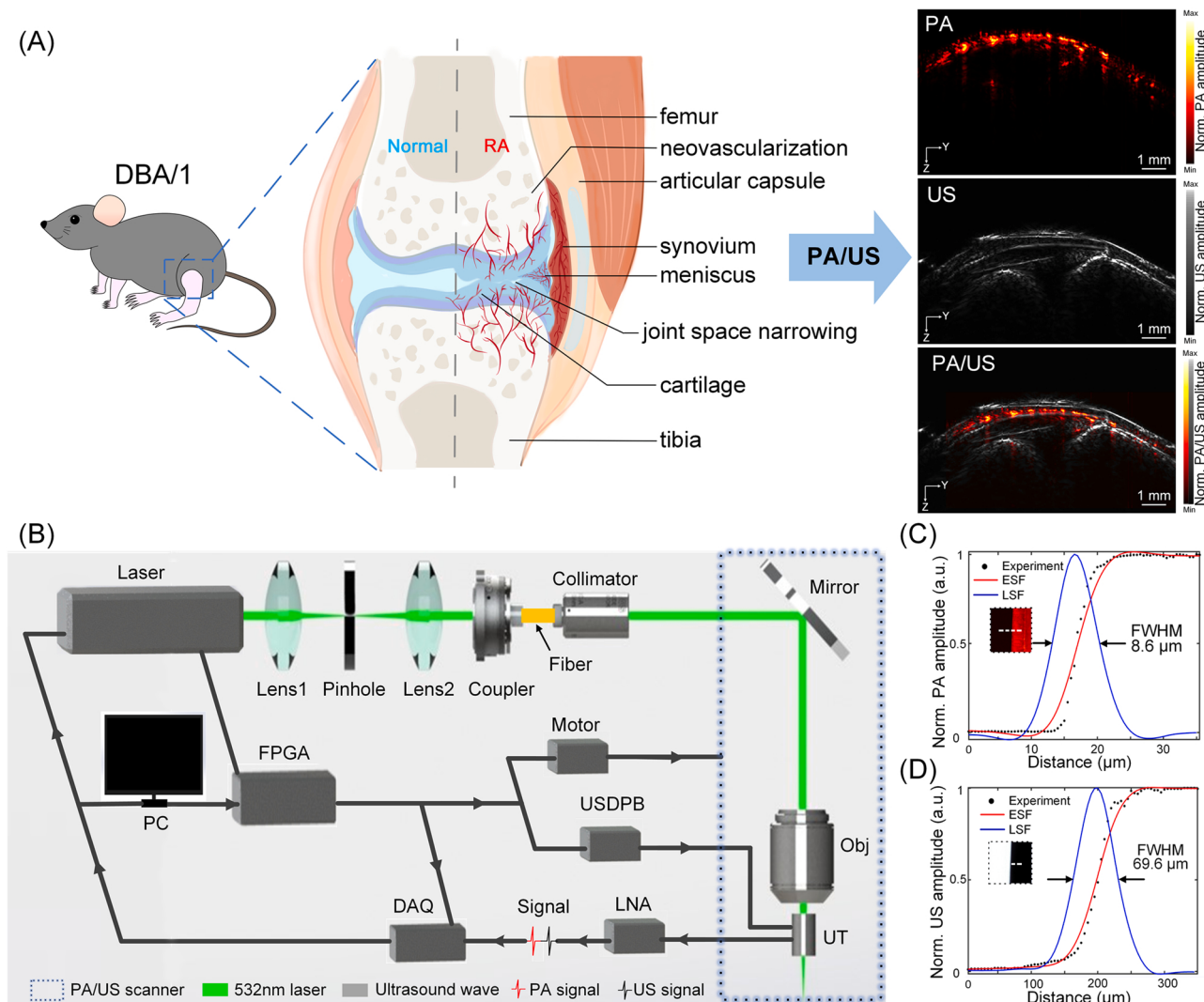


Fig. 1. Schematic diagram of RA pathology, imaging modality and the PA/US system. (A) Schematic diagram of rheumatoid arthritis knee lesions and imaging modalities. The principal pathological changes in rheumatoid arthritis are vascular opacification, synovial erosion and cartilage destruction, accompanied by inflammatory cell infiltration and the release of large amounts of cytokines. Images of the PA/US dual-modality system on the knee joint of an RA mouse are also shown, with PA images, US images and PA/US coupled images. (B) Optical and circuit connections of the PA/US system. (C) The lateral resolution of PA imaging measured with the sharp-edge method. (D) The lateral resolution of US imaging measured with the sharp-edge method. FPGA, field-programmable gate array; USDPB: ultrasound transducer delay pause board; DAQ, data acquisition; LNA, low noise amplifier; Obj, Objective; UT, ultrasound transducer.

ankles) was determined by a subjective grading system (Table 1). A clinical severity score of 0–4 was assigned to each joint [52]. According to the observed experimental results, we grade the photoacoustic signals of the blood vessels in the knee joints of RA mice under photoacoustic/ultrasound, we scored angiogenesis according to normal and four different disease grades, the area and shape of color pixels in the knee joint area, the results are shown in Table 2.

Table 1
Scoring system for subjective evaluation of arthritis severity.

Severity score	Degree of inflammation
0	No signs of erythema or swelling
1	Erythema and mild swelling confined to the tarsal or ankle joint
2	Erythema and mild swelling from the ankle to the tarsus
3	Erythema and moderate swelling from the ankle to the metatarsophalangeal joint
4	Erythema and severe swelling including ankles, feet and fingers, or toxicity of extremities

Table 2
Photoacoustic RA neovascularization severity scoring system.

Severity score	Degree of inflammation
0	No or very few point detectable PA signals
1	2–3 points or small patches of detectable PA signal
2	3–4 points or small patches of detectable PA signal
3	2–3 wide linear detectable PA signals extending to the center of the joint cavity
4	The PA signal area extends in large contiguous patches to the center of the joint cavity

2.2.2. Histological analysis

After imaging was completed, mice were euthanized, hind limbs were separated from the hip joint, fixed using paraformaldehyde and decalcified using ethylenediaminetetraacetic acid (EDTA), and used for histological studies. Histological analysis plays a key role in the assessment of rheumatoid arthritis of the knee joints, and microscopic images are used to demonstrate the underlying morphology of bone and

cartilage fibers, useful for corroborating photoacoustic imaging results [30].

2.3. Multimodal PA/US imaging system

In this study, the schematic diagram of the PA/US microscopy system is shown in Fig. 1(B). Briefly, the excitation source of the PA signal is a

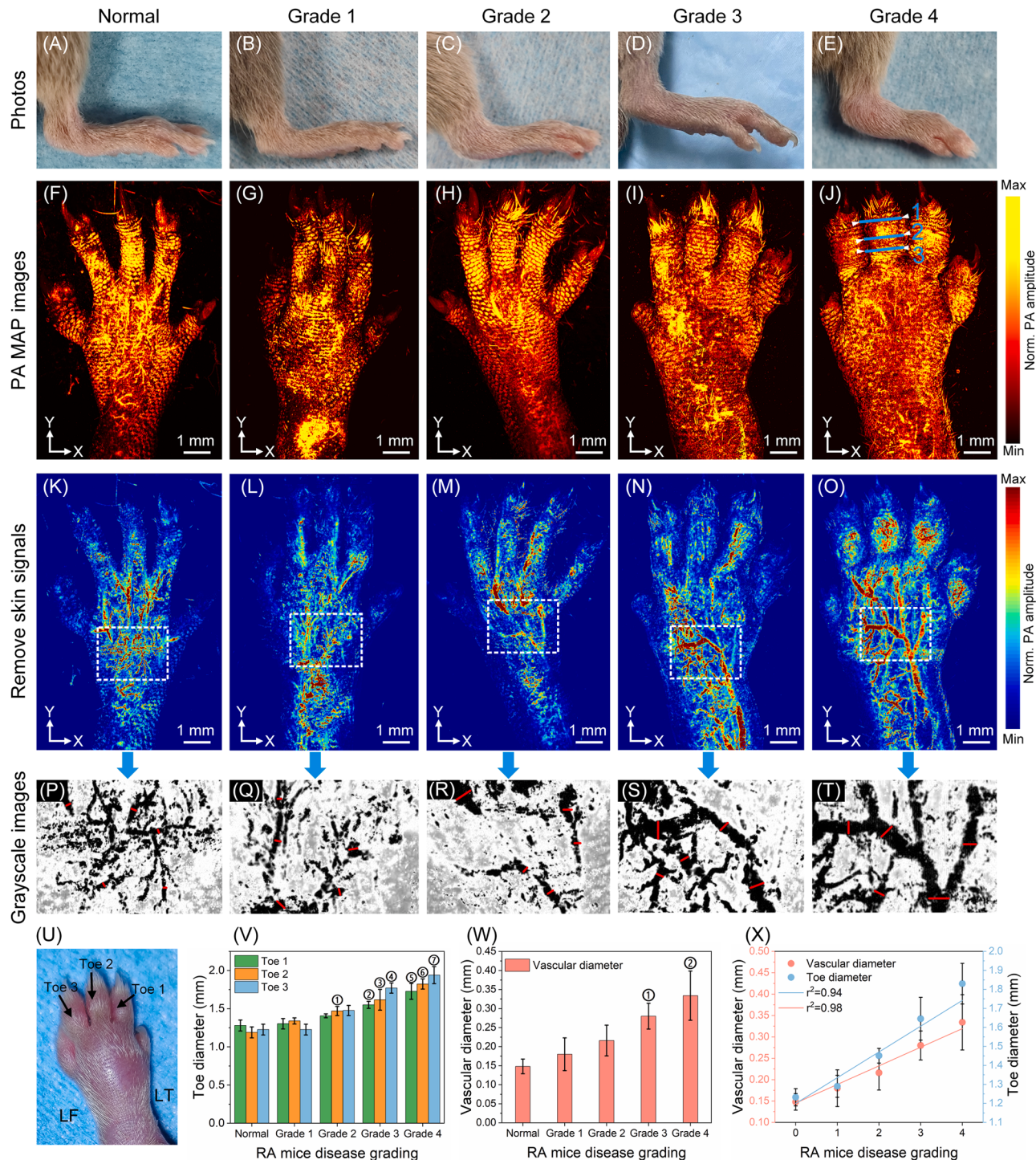


Fig. 2. Photoacoustic imaging of the hind paws of DBA/1 mice. (A–E) Macrophotographs of the hind paws of normal and grade 1–4 RA mice. (F–J) Maximum amplitude projection (MAP) imaging of the hind paws of normal and grade 1–4 RA mice. (K–O) Maximum amplitude projection imaging after removing the skin signal to expose the internal vasculature, which can reflect the extent of the disease. (P–T) Grayscale map of the hind paw of a mouse to provide a better picture of the vascular pathways and morphology. (U) Top view of the hind paw of a DBA/1 mouse (left). (V) Different toe diameters of the hind paws of RA mice with different disease states were counted, and each toe was measured at three different positions: upper, middle and lower (1,2,3). n = 3, ①p = 0.027, ②p = 0.014, ③p = 0.001, ④p < 0.0001, ⑤p < 0.0001, ⑥p < 0.0001, ⑦p < 0.0001, ⑧p = 0.001, ⑨p < 0.0001, ⑩p < 0.0001. (W) The diameters of subcutaneous blood vessels in the hind paws of RA mice with different disease states were counted and measured at five locations. n = 3, ①p = 0.001, ②p < 0.0001. (X) Correlation analysis of RA disease classification with vessel diameter ($r^2 = 0.98$) and toe diameter ($r^2 = 0.94$). PA MAP, photoacoustic maximum amplitude projection; LF, lateral fibula ; LT, lateral tibial.

nanosecond pulsed laser with a wavelength of 532 nm (DTL-314qt, Russian Laser Export; pulse width of 7 ns and repetition rate of 5 kHz). The beam was coupled to a single-mode fiber through a fiber coupler (paf-x-7-a, Thorlabs). The single-mode fiber guides the laser beam, which is then reflected by a biaxial oscillator scanner (s8107, Century Sunny, China) and finally focused by a $4 \times$ objective (gco-2111, Daheng Optical, China) to excite the PA signal. A homemade ultrasonic transducer with a center frequency of 25 MHz, bandwidth of over 90 %, diameter of 8 mm, and 3 mm hole in the center as the laser beam exit was used for photoacoustic detection. As shown in Fig. 1(C) and(D), the lateral resolution of PA imaging was 8.6 μm and the lateral resolution of US imaging was 69.6 μm . Deionized water was used as a coupling agent to couple the imaging area of the mouse knee joint to the transducer. The imaging range was $10 * 10 \text{ mm}^2$, the scanning speed was 10 mm/s, and the step size was 8 μm for the X-axis and 10 μm for the Y-axis. Simultaneously, the laser excited the scanning system and the data acquisition system simultaneously. The acquired PA signals were amplified by an amplifier (50 dB gain, LNA-650, RF Bay, USA) and the amplified PA signal was digitized by a data acquisition card (250 MS/s, m3i.3221, Spectrum, Germany). The scanning system and the acquisition system were driven by linear motors. Each laser pulse produced an A-line signal in the one-dimensional depth direction. At the same time, a 2D transverse scan obtained 3D data information constructed from the A-line signal, and the PA/US signal was reconstructed by an algorithm to obtain the PA/US image information of the knee joint from the superficial to the deeper layers.

2.4. Statistical analysis

One-way analysis of variance (ANOVA) was performed using Bonferroni post hoc test to compare data from multiple samples, significance level was set at $P < 0.05$, and all data were expressed as mean \pm standard deviation (SD), using SPSS 27.0 software (SPSS Inc. Chicago, IL).

3. Results

We first obtained photoacoustic images of the mouse hind paw [Fig. (2)]. Our system could distinguish the intensity and range of the photoacoustic signals of the hind paw at various stages of the disease, allowing us to analyze the internal vascular diameter of the paw, and the degree of swelling of the paw. Fig. 2(A)–(E) show macrophotographs of the hind paw of normal DBA/1 mice and mice with scores 1–4, respectively, a result based on the subjective grading system as described in the Methods section. Fig. 2(F)–(J) show PA maximum amplitude projection (MAP) images demonstrating the hind paw morphology of the mice, such as toe diameter, scale arrangement, and density of the skin surface and superficial skin vessels. The RA mice with a score of 4 have a significantly increased toe diameter compared to normal mice, which is consistent with the subjective grading system score, and there is swelling throughout the hind paw. RA mouse with a score of 4 has the most severe disease state, with severe swelling and erythema on the feet. The amplitude of photoacoustic signal on skin surface is relatively large, so no obvious vascular tree can be observed in the MAP image. Only after removing the strong signal on the skin surface, more blood vessels appear in Fig. 2O. We focused on the toe diameters and counted the diameters of the second to fourth toe [Fig. 2(U)], which were repeatedly measured three times for each toe in the upper middle and lower positions as in Fig. 2(J). The corresponding quantitative results [Fig. 2(V)], show that the toes 1–3 diameters of mice increased with the increase of RA disease score. As the disease fraction of the mice increased, so did their toe diameter, and the disease scores were closely correlated with toe diameter ($r^2 = 0.94$) [Fig. 2(X)]. In addition, to show the physiological status and morphology of the subcutaneous blood vessels as well, the PA images after removing the skin surface were performed [Fig. 2(K)–(O)]. Similarly, the subcutaneous vessels of mice with a score of 4

have significantly wider diameter and richer photoacoustic signals, such as in Fig. 2(O), which can clearly distinguish the morphology, alignment and photoacoustic signal intensity of the subcutaneous vessels. We selected essentially the same area of the hind paw of mice with different RA grades (e.g., the white rectangular area in Fig. 2(K)–(O) and performed threshold-based segmentation of this area to highlight the vascular morphology [Fig. 2(P)–(T)]. In this image, the morphology of the vessels can be clearly observed, for which we selected the major vessels in each image, a total of five loci (e.g., the short red line in Fig. 2 (P)–(T)) for statistical analysis [Fig. 2(W)], from which it shows that an increase in vessel diameter correlates with an increase in score level ($r^2 = 0.98$) [Fig. 2(X)].

More importantly, we carried out photoacoustic imaging of knee joints in normal and RA mouse models with different RA grades. Fig. 3 shows the PA imaging results of knee joints in DBA/1 mice. Fig. 3(A)–(E) shows the PA MAP results of the knee joint in different disease states. Due to individual differences in mice, the maximum projection information of knee joint is different, but the great saphenous vein (the thicker blood vessels at the bottom of the figure) can be clearly imaged, demonstrating the imaging resolution and imaging depth of our system. The XZ cross-sectional MAP images of fifty continuous PA B-mode images at the dotted line position are shown in Fig. 3(F)–(J). In the photoacoustic signal inside the knee joint (the area outlined by the white dotted line), the photoacoustic signal intensity and signal area, in the knee joint of the RA mouse, increase with the increase in disease score compared with the normal mouse [Fig. 3(V)]. We also processed the photoacoustic information of the YZ cross-sectional MAP images [Fig. 3 (K)–(O)]. The photoacoustic signal intensity and area of the YZ cross section were also quantitatively analyzed [Fig. 3(W)]. The location of the photoacoustic signal within the knee joint in the YZ section (the area outlined by the white dashed line) is the same as that in the XZ section. The intensity of the photoacoustic signal and the volume of the signal area within the knee joint were increased compared to normal mice.

However, it is worth noting that we used a square ($10 \text{ mm} * 10 \text{ mm}$) image acquisition area for photoacoustic signal acquisition. Interestingly, the YZ section seems to have a larger photoacoustic signal area than the XZ section. We think this is related to the morphology of the new pannus in the RA knee joint, and is worthy of further exploration. Fig. 3(P)–(T) shows depth-encoded horizontal-sectional images of normal and different RA disease scores knee joint. We performed image reconstruction for different depths of the knee joint, for RA mice, were able to find significant vascular photoacoustic signals at 1.5–2.1 mm in depth [Fig. 3(Q)–(T)], and the area of photoacoustic signals in the knee joint of RA mice increased with increasing disease score compared to normal mice [Fig. 3(P)]. In order to visualize the photoacoustic signal within the knee joint more visually, as in Fig. 3(U) we built a 3D image of the mouse knee joint with a score of 4. The photoacoustic signal of the skin (indicated by the black arrow) can be clearly distinguished, and a distinct vascular opacification in the photoacoustic signal is visible below the skin signal (black dashed circle ROI area in Fig. 3(U)). This clearly illustrates the imaging capability and quality of our system for RA knee vascular opacification.

The B-mode observation of the knee joint is shown in Fig. 4(A)–(E). The triangular area consisting of the tibiofemoral tendon (dark hyperechoic area parallel to the skin surface), tibia and femur (red triangular area in Fig. 4(F)) is defined as the TTF (tibiofemoral tendon-tibia-femur). Fig. 4(F) shows that the TTF area in normal mice is a homogeneous and bright acute triangular area with no significant synovial erosion or bone destruction. Fig. 4(G)–(J) are B-mode US imaging results of the knee joint of DBA/1 RA mice with scores of 1–4, respectively. As shown in Fig. 4(G), the low echo area attached to the surface of the femur and tibia can be seen in the TTF area of mice with a score of 1 (green area in the figure, determined by Pair software), and shows diffuse synovial edema. Fig. 4(H) shows that in the TTF area of mice with an RA score of 2, the hypoechoic area further expands along the bone surface and tends to extend to the center of the TTF area. Mode B of the

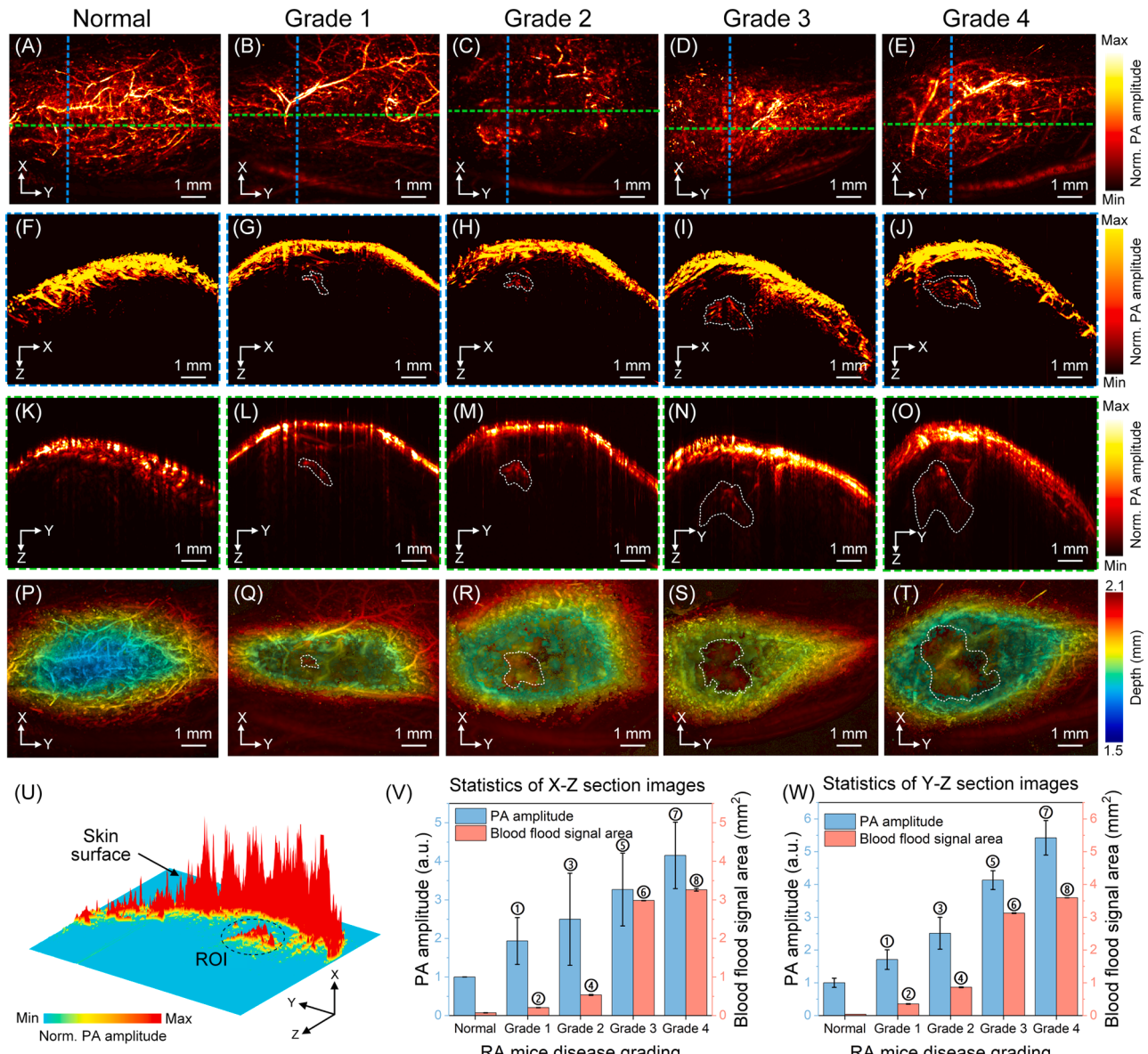


Fig. 3. In vivo imaging of the knee joint in DBA/1 mice. (A–E) XY-plane maximum projections of in vivo photoacoustic imaging of the knee joint in DBA/1 mice. (F–J) XZ-plane cross-sections of photoacoustic imaging of DBA/1 mice with different degrees of disease. (K–O) Photoacoustic YZ-plane cross-sections of DBA/1 mice with different degrees of disease. (P–T) Depth-coded images of DBA/1 mice with different degrees of disease in the XY plane at 1.5–2.1 mm. (U) Three-dimensional image of the knee joint of a mouse with a score of 4. (V) Statistical maps of photoacoustic signal intensity and blood flow signal areas in X-Z plane. n = 3, ①p < 0.0001, ②p < 0.0001, ③p < 0.0001, ④p < 0.0001, ⑤p < 0.0001, ⑥p < 0.0001, ⑦p < 0.0001. (W) Statistical maps of photoacoustic signal intensity and blood flow signal areas in X-Z plane. n = 3, ①p < 0.0001, ②p < 0.0001, ③p < 0.0001, ④p < 0.0001, ⑤p < 0.0001, ⑥p < 0.0001, ⑦p < 0.0001, ⑧p < 0.0001.

knee joint of mice with score of 3 is shown in Fig. 4(I). There is a low echo area with obvious expansion toward the center, and the density of the low echo area is higher than that of mice with scores of 1–2. Fig. 4(J) shows the B-mode image of a mouse knee joint with a score of 4. In the disease state with this score, the TTF area is significantly expanded and is basically filled with TTF area, with the remaining area only comprising a small part. The results of the hypoechoic area were counted and displayed in Fig. 4(K), and the correlation between the area and the grading was analyzed. Compared with normal mice, the hypoechoic area increased with the grading ($r^2 = 0.87$) [Fig. 4(L)]. Knowing the proportion of synovial erosion area helps to grade the disease, as shown in Fig. 4(M), which demonstrates the proportion of hypoechoic areas in the TTF area due to synovial erosion. While RA will lead to joint narrowing, knowing the length of the joint gap will help to better grasp

the disease status. Measuring the joint gap length in mice with different disease grades indicated that the joint gap length and the disease grade roughly showed a negative correlation ($r^2 = 0.84$) [(Fig. 4(N) and (O)].

The results of the PA/US dual-mode imaging are presented in Fig. 5 (A)–(E). On the bimodal imaging results, localization by B-mode delineates the TTF region (blue triangular area in Fig. 5(A)–(E)), within which the photoacoustic signal is visible (red area). In photoacoustic image of the normal mouse, a very small amount of punctate photoacoustic signal can be seen within the TTF region [Fig. 5(A)]. In the RA mouse, two to three larger areas of punctate photoacoustic signal attached to the femoral and tibial joint surfaces can be seen within the TTF region in mice with a score of 1. In mice with a score of 2, more areas of dotted lamellar photoacoustic signals can be seen in the TTF area attached to the femoral and tibial articular surfaces. In mice with a

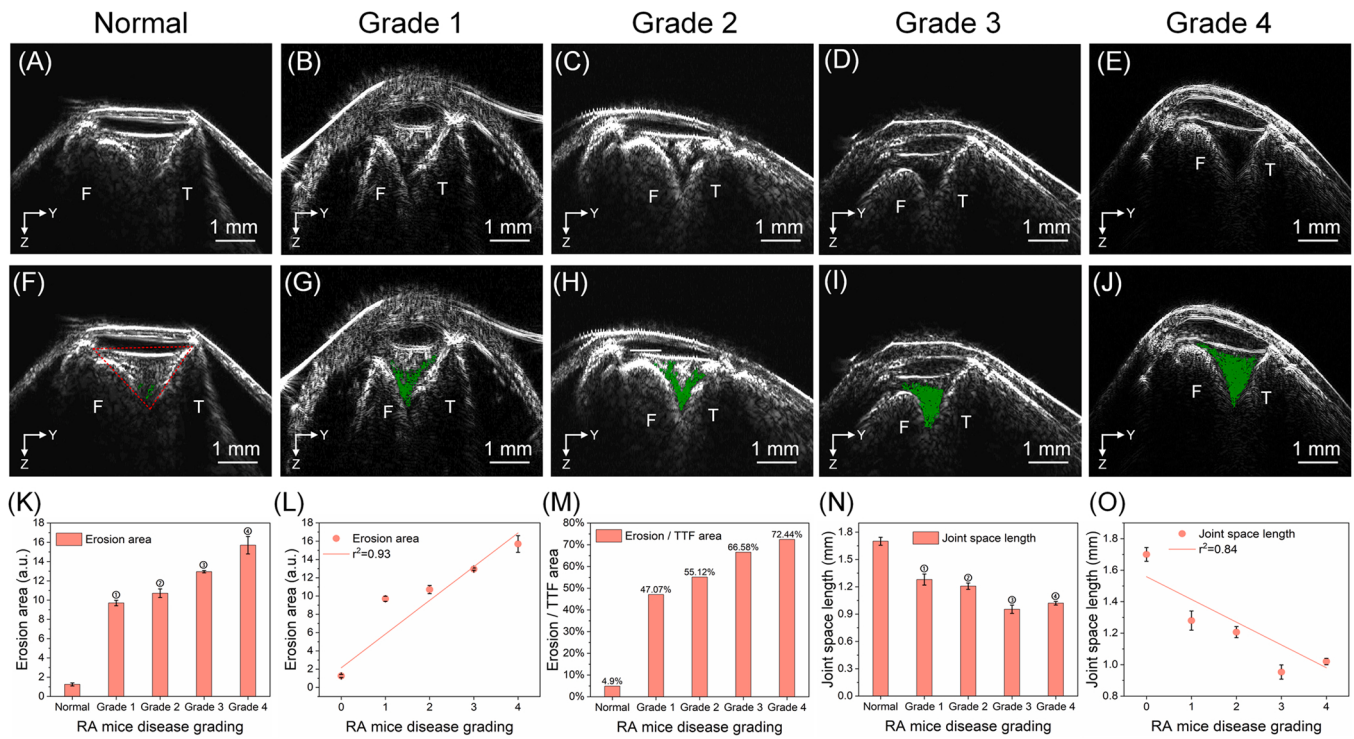


Fig. 4. B-mode images of ultrasound showing synovial erosion in the joint cavity. (A) DBA/1 ultrasound of a normal mouse knee joint showing articular cavity morphology. (B) Score 1 DBA/1 ultrasound of joint cavity morphology. (C) Score 2 DBA/1 ultrasound joint cavity pattern. (D) Score 3 DBA/1 ultrasound joint cavity pattern. (E) Score 4 DBA/1 ultrasound joint cavity pattern. (F–J) B-scan images showing synovial erosion. The green area is a low signal area due to synovial erosion. (K–L) Statistical results of synovial erosion area in the joint cavity with different disease scores and correlation between erosion area and score ($r^2 = 0.93$). n = 5, ①p < 0.0001, ②p < 0.0001, ③p < 0.0001, ④p < 0.0001. (M) Proportion of synovial erosion area in the TTF area. (N–O) Statistical results of joint cavity gap length with different disease scores and correlation between joint cavity gap length and scores ($r^2 = 0.84$). n = 3, ①p < 0.0001, ②p < 0.0001, ③p < 0.0001, ④p < 0.0001. F: femur; T: tibia; TTF: tibiofemoral tendon-tibia-femur.

score of 3, linear areas of photoacoustic signal along the femoral and tibial joint surfaces can be seen in the TTF region. In mice with a score of 4, a patchy area of photoacoustic signal extending toward the center of the joint cavity can be seen in the TTF area.

The results of H&E staining were demonstrated in Fig. 5(F)–(J). As shown in the H&E stained images, mice with scores of 1 and 2 have less severe disease and a more normal knee joint space, but mice with a score of 3 and 4 have a significantly narrower knee joint space. Compared with normal mice, the neovascularization in the synovium, meniscus and subchondral bone gradually increased in the RA mouse model. Fig. 5(K) shows the TTF region map of normal and RA mice. Compared with normal mice, the photoacoustic signal region area of RA mice increases with the increase of disease score. We calculated the area of the photoacoustic signals, which reflects the extent of pannus in the knee joint [Fig. 5(L)]. Fig. 5(L) also shows the intensity of the photoacoustic signal, which reflects the density, diameter, and flow of blood vessels. The area and intensity of the photoacoustic signal are positively correlated with disease score, as shown in Fig. 5(M). Compared with the photoacoustic signal area ($r^2 = 0.82$), the photoacoustic signal intensity seems to be able to better predict the severity of disease ($r^2 = 0.98$).

4. Discussion

The diagnosis and monitoring of RA in animals currently relies on subjective scoring and pathological examination. Subjective scoring is subject to human factors, and pathological examinations are invasive and invasive and cannot be used for long-term monitoring purposes [19, 30]. The need for safer and more convenient diagnostic and monitoring methods is particularly urgent.

Herein, we report a study using PA/US dual-mode system to image pannus, joint structures, and cartilage in the knee joint of a DBA/1

mouse model of RA. Compared with previously reported findings, our imaging results have higher resolution and more precise localization of the photoacoustic signal [29, 43]. Increased hind paw vessel diameter stimulated by inflammatory factors, increased hind paw thickness and hind paw toe diameter are characteristic lesions of RA. We quantified blood vessel diameter and hind paw toe diameter under PA and US, and correlated blood vessel diameter and toe diameter of hind paw with the disease grade of mice. As far as we know, this has not been reported before. Compared with the previously reported subjective assessment scoring system for arthritis severity, we achieved a quantitative analysis of joint and toe deformities caused by RA, excluding human subjective factors, and a more accurate grading of RA in mice. This study focused on the photoacoustic imaging of pannus and ultrasonic imaging of joint structure of the knee joint. The synovial blood vessels proliferating in the knee joint of RA mice are rich in hemoglobin. Hemoglobin, a natural photoacoustic imaging agent, has a high absorption peak near 532 nm, which enables us to render the signal of vascular opacities well without additional contrast agent. In the RA model, pannus persists and develops through the supply of inflammatory cells, cytokines and nutrients in the synovium. After CIA induction, the number of new blood vessels in the synovium will increase with time. Vascularization is also associated with the severity of arthritis and can be assessed by subjective assessment scoring system or histological scores. However, the strength of the PA signal mainly depends on the concentration of hemoglobin in the blood vessels. The PA signal represents the difference in the number and density of synovial hyperplasia and new blood vessels, the range of blood flow signals detected in photoacoustic imaging will reflect the severity of the disease which is verified on the HE slices in Fig. 5(F)–(J). However, due to the limited imaging depth of the 532 nm laser, our results can only show approximate photoacoustic signals in the TTF area, and cannot quantitatively analyze vascular morphology, such as

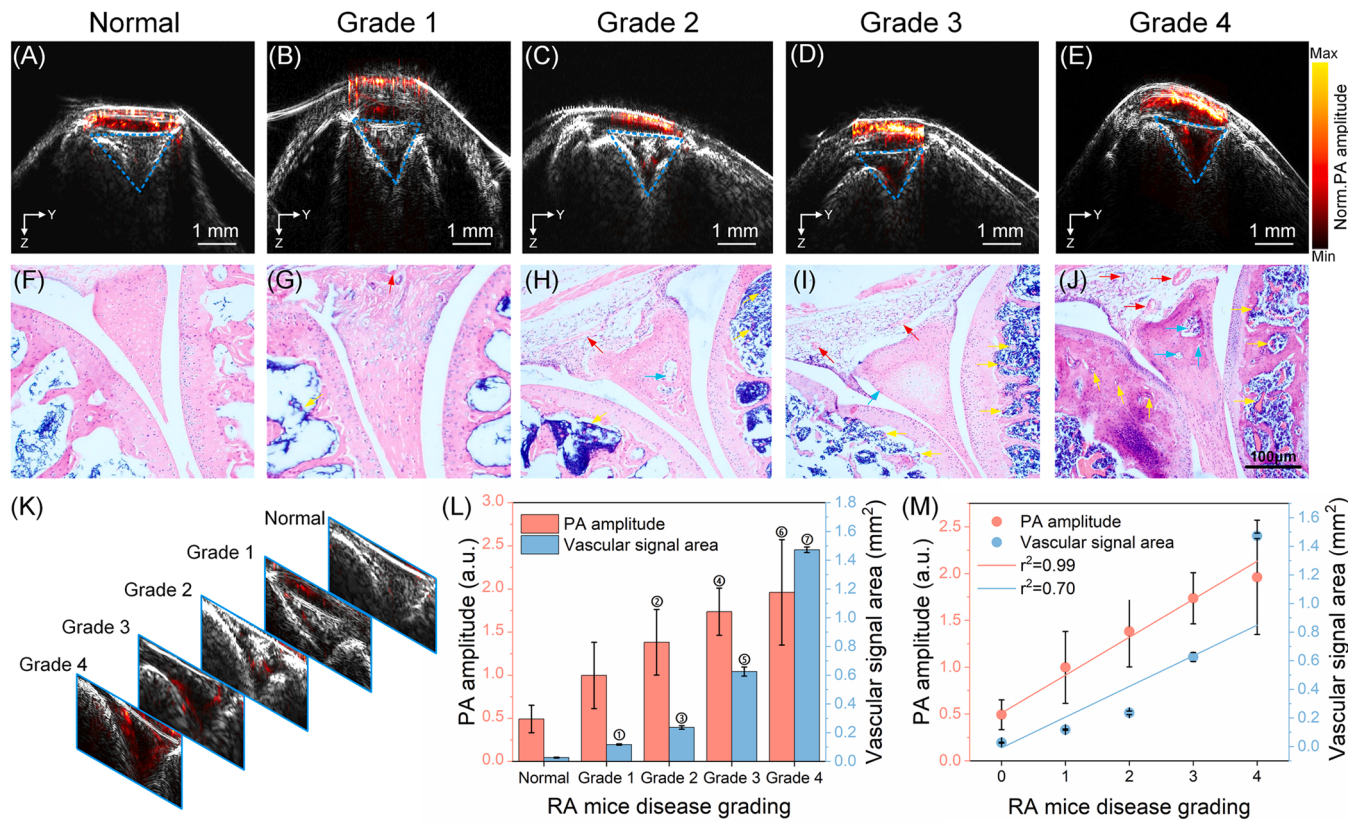


Fig. 5. Photoacoustic-ultrasound dual-mode examination of the knee joint in RA DBA/1 mice. (A–E) Photoacoustic sonograms of the knee joint in RA DBA/1 mice in normal and different disease states. (F–J) H&E staining of knee joints in normal and RA mice. All the scale bar is 100 μ m. Red arrow: neovascularization in the synovial membrane; Blue arrow: neovascularization in the meniscus; Yellow arrow: neovascularization in subchondral bone. (K) PA/US dual-modality imaging result maps of the TTF region of the knee joint in mice with different disease states. (L) Photoacoustic signal intensity and blood flow signal area of TTF region in mice with different disease states. $n = 5$, $\oplus p = 0.001$, $\ominus p = 0.018$, $\ominus\ominus p < 0.0001$, $\ominus\ominus\ominus p = 0.001$, $\ominus\ominus\ominus\ominus p < 0.0001$, $\ominus\ominus\ominus\ominus\ominus p < 0.0001$. (M) Correlation of photoacoustic signal intensity ($r^2 = 0.99$) and blood flow signal area ($r^2 = 0.70$) with disease scores in the TTF region of mice.

diameter and curvature. We have previously reported surprising results using a 532/1064 nm dual wavelength laser imaging system for full skin imaging [20]. The 532/1064 nm dual wavelength may be able to compensate for the current shortcomings and achieve deeper and more accurate photoacoustic imaging of RA vascular opacities.

During RA progression, the synovium undergoes pathological changes that cannot be ignored [53]. The synovium is the main target of inflammation in RA, and it has been demonstrated that the RA synovium exhibits proliferation and neovascularization, which is thought to be accompanied by abnormal production of immune cell accumulation; it is mainly promoted by cytokines, growth factors, and hypoxia-inducing factors secreted by macrophages and fibroblasts involved in the synovium; as the abnormal neovascularization is at an immature stage, it allows leukocytes to migrate, which leads to the transformation of the neovascularization into an aggressive vascular opacity that damages articular cartilage and bone [54,55]. Limited by the imaging capability of single-array ultrasound, cartilage and bone damage cannot be clearly demonstrated, but cartilage and bone damage can be judged by the discontinuity and signal intensity of the bone. The aggressive opacities show up as low signal areas in B-mode imaging. Based on the low echo area between femur and tibia, as shown in Fig. 4(A)–(E), allows us to make quantitative analysis of synovial hyperplasia and erosion. B-mode reflects the state of the synovium, and the B-mode score has good correlation with the subjective scoring system, this will allow local assessment of the disease state by ultrasound, which is well confirmed by HE staining [Fig. 5 (F) and (J)].

5. Conclusion

In conclusion, our results have demonstrated that PA/US dual-mode imaging is a valuable method for assessing RA lesions in mice. PA offers the advantage of visualizing and analyzing the neovascularization within the RA knee, and US can also quantify erosive vascular opacities within the knee joint. This study has not only provided more tools and possibilities for the research of RA mouse models, but also assisted the evaluation of potential drugs.

CRediT authorship contribution statement

Z.W., Z.T., G.N., J.H., B.Y., Z.W., J. H., W. L. conceived the experimental design and participated in most of the experiments, Z.W., E.W., H.C., Z. W., J.H. participated in the data analysis and wrote the main manuscript text. E.W., B.Y. participated in the data analysis code writing and the ultrasonic transducer fabrication. All authors read and approved the final version of the manuscript.

Declaration of Competing Interest

The authors declare that they have no known competing financial interests or personal relationships that could have appeared to influence the work reported in this paper.

Data Availability

Data will be made available on request.

Acknowledgements

This work was supported by the Guangdong Basic and Applied Basic Research Foundation (2021A1515011285, 2019A1515010800), Major Project under the Science and Technology Development Scheme of Guangdong Province (210715106900918, [2020]53-129), Li Ka Shing Foundation Cross-Disciplinary Research Grant (2020LKSFG03A), and Shantou Science and Technology Plan Medical And Health Category Project (211114216492935).

References

- [1] S. Jang, E.J. Kwon, J.J. Lee, Rheumatoid arthritis: pathogenic roles of diverse immune cells, *Int. J. Mol. Sci.* 23 (2) (2022).
- [2] I.B. McInnes, G. Schett, The pathogenesis of rheumatoid arthritis, *N. Engl. J. Med.* 365 (23) (2011) 2205–2219.
- [3] L.D. Kumar, R. Karthik, N. Gayathri, T. Sivasudha, Advancement in contemporary diagnostic and therapeutic approaches for rheumatoid arthritis, *Biomed. Pharm.* 79 (2016) 52–61.
- [4] P.E. Lazzerini, P.L. Cappelli, F. Laghi-Pasini, Systemic inflammation and arrhythmic risk: lessons from rheumatoid arthritis, *Eur. Heart J.* 38 (22) (2017) 1717–1727.
- [5] E. Filippucci, et al., Ultrasound imaging in rheumatoid arthritis, *Radiol. Med.* 124 (11) (2019) 1087–1100.
- [6] I.B. McInnes, J.R. O'Dell, State-of-the-art: rheumatoid arthritis, *Ann. Rheum. Dis.* 69 (11) (2010) 1898–1906.
- [7] S. Jagannathan, et al., Spectrum of synovial pathologies: a pictorial assay, *Curr. Probl. Diagn. Radiol.* 41 (1) (2012) 30–42.
- [8] C.B. Chung, R. Boucher, D. Resnick, MR imaging of synovial disorders of the knee, *Semin. Musculoskelet. Radiol.* 13 (4) (2009) 303–325.
- [9] R. Knevel, et al., Evaluating joint destruction in rheumatoid arthritis: is it necessary to radiograph both hands and feet? *Ann. Rheum. Dis.* 72 (3) (2013) 345–349.
- [10] A. Barile, et al., Computed tomography and MR imaging in rheumatoid arthritis, *Radiol. Clin.* 55 (5) (2017) 997–1007.
- [11] H. Sugimoto, Imaging of rheumatoid arthritis: role of MR imaging and CT, *Nihon Rinsho* 71 (7) (2013) 1193–1197.
- [12] A. Stewart, L.M. Mackenzie, A.J. Black, D.M. Reid, Predicting erosive disease in rheumatoid arthritis. A longitudinal study of changes in bone density using digital X-ray radiogrammetry: a pilot study, *Rheumatology* 43 (12) (2004) 1561–1564.
- [13] P.C. Taylor, The value of sensitive imaging modalities in rheumatoid arthritis, *Arthritis Res. Ther.* 5 (5) (2003) 210–213.
- [14] T. Norimura, S. Nomoto, M. Katsuki, Y. Gondo, S. Kondo, p53-dependent apoptosis suppresses radiation-induced teratogenesis, *Nat. Med.* 2 (5) (1996) 577–580.
- [15] C.G. Borrero, J.M. Mountz, J.D. Mountz, Emerging MRI methods in rheumatoid arthritis, *Nat. Rev. Rheumatol.* 7 (2) (2011) 85–95.
- [16] U.M. Döhn, et al., Rheumatoid arthritis bone erosion volumes on CT and MRI: reliability and correlations with erosion scores on CT, MRI and radiography, *Ann. Rheum. Dis.* 66 (10) (2007) 1388–1392.
- [17] K. Dantendorfer, D. Wimberger, H. Katschnig, H. Imhoff, Claustrophobia in MRI scanners, *Lancet* 338 (8769) (1991) 761–762.
- [18] N. Beziere, et al., Optoacoustic imaging and staging of inflammation in a murine model of arthritis, *Arthritis Rheumatol.* 66 (8) (2014) 2071–2078.
- [19] D. Chamberland, Y. Jiang, X. Wang, Optical imaging: new tools for arthritis, *Integr. Biol.* 2 (10) (2010) 496–509.
- [20] Z. Wang, et al., Bifocal 532/1064 nm alternately illuminated photoacoustic microscopy for capturing deep vascular morphology in human skin, *J. Eur. Acad. Dermatol. Venereol.* 36 (1) (2022) 51–59.
- [21] Z. Wang, et al., Photoacoustic-guided photothermal therapy by mapping of tumor microvasculature and nanoparticle, *Nanophotonics* 10 (12) (2021) 3359–3368.
- [22] D. Cui, Y. Shi, D. Xing, S. Yang, Ultrahigh sensitive and tumor-specific photoacoustography in NIR-II region: optical writing and redox-responsive graphic fixing by AgBr@PLGA nanocrystals, *Nano Lett.* 21 (16) (2021) 6914–6922.
- [23] S. Cho, J. Baik, R. Managuli, C. Kim, 3D PHOVIS: 3D photoacoustic visualization studio, *Photoacoustics* 18 (2020), 100168.
- [24] P. Beard, Biomedical photoacoustic imaging, *Interface Focus* 1 (4) (2011) 602–631.
- [25] L.V. Wang, S. Hu, Photoacoustic tomography: in vivo imaging from organelles to organs, *Science* 335 (6075) (2012) 1458–1462.
- [26] M. Omar, J. Aguirre, V. Ntziacharistos, Optoacoustic mesoscopy for biomedicine, *Nat. Biomed. Eng.* 3 (5) (2019) 354–370.
- [27] Q. Fu, R. Zhu, J. Song, H. Yang, X. Chen, Photoacoustic imaging: contrast agents and their biomedical applications, *Adv. Mater.* 31 (6) (2019), e1805875.
- [28] L. Xi, H. Jiang, High resolution three-dimensional photoacoustic imaging of human finger joints in vivo, *Appl. Phys. Lett.* 107 (6) (2015), 063701.
- [29] J. Chen, et al., Tocilizumab-conjugated polymer nanoparticles for NIR-II photoacoustic-imaging-guided therapy of rheumatoid arthritis, *Adv. Mater.* 32 (37) (2020), 2003399.
- [30] Y. Lin, et al., Molecular photoacoustic imaging for early diagnosis and treatment monitoring of rheumatoid arthritis in a mouse model, *Am. J. Transl. Res.* 13 (8) (2021) 8873.
- [31] M. Østergaard, S. Møller-Bisgaard, Rheumatoid arthritis: is imaging needed to define remission in rheumatoid arthritis? *Nat. Rev. Rheumatol.* 10 (6) (2014) 326–328.
- [32] C.G. Peterfy, New developments in imaging in rheumatoid arthritis, *Curr. Opin. Rheumatol.* 15 (3) (2003) 288–295.
- [33] M. Jain, J. Samuels, Musculoskeletal ultrasound as a diagnostic and prognostic tool in rheumatoid arthritis, *Bull. NYU Hosp. Jt. Dis.* 69 (3) (2011) 215–219.
- [34] T. Funck-Brentano, et al., Benefits of ultrasonography in the management of early arthritis: a cross-sectional study of baseline data from the ESPOIR cohort, *Rheumatology* 48 (12) (2009) 1515–1519.
- [35] S. Ohrndorf, M. Backhaus, Advances in sonographic scoring of rheumatoid arthritis, *Ann. Rheum. Dis.* 72 Suppl 2 (2013) ii69–ii75.
- [36] K. Ben Abdelghani, et al., Role of ultrasound in assessing remission in rheumatoid arthritis, *Diagn. Inter. Imaging* 96 (1) (2015).
- [37] L. Casimiro, et al., Therapeutic ultrasound for the treatment of rheumatoid arthritis, *Cochrane Database Syst. Rev.* 3 (2002), CD003787.
- [38] W. Li, et al., Mutual-reinforcing sonodynamic therapy against Rheumatoid Arthritis based on sparfloxacin sonosensitizer doped concave-cubic rhodium nanozyme, *Biomaterials* 276 (2021), 121063.
- [39] Z. Cheng, et al., An excitation-reception collinear probe for ultrasonic, photoacoustic, and thermoacoustic tri-modal volumetric imaging, *IEEE Trans. Med. Imaging* 40 (12) (2021) 3498–3506.
- [40] H. Guo, et al., Assessing the development and treatment of rheumatoid arthritis using multiparametric photoacoustic and ultrasound imaging, *J. Biophotonics* 12 (11) (2019), e201900127.
- [41] J. Jo, et al., Photoacoustic tomography for human musculoskeletal imaging and inflammatory arthritis detection, *Photoacoustics* 12 (2018) 82–89.
- [42] J. Jo, et al., A functional study of human inflammatory arthritis using photoacoustic imaging, *Sci. Rep.* 7 (1) (2017) 15026.
- [43] J.R. Rajian, X. Shao, D.L. Chamberland, X. Wang, Characterization and treatment monitoring of inflammatory arthritis by photoacoustic imaging: a study on adjuvant-induced arthritis rat model, *Biomed. Opt. Express* 4 (6) (2013) 900–908.
- [44] S. Drevet, B. Favier, B. Lardy, G. Gavazzi, E. Brun, New imaging tools for mouse models of osteoarthritis, *GeroScience* 44 (2) (2022) 639–650.
- [45] Z. Liu, et al., Photoacoustic imaging of synovial tissue hypoxia in experimental post-traumatic osteoarthritis, *PBMB* 148 (2019) 12–20.
- [46] J. Chen, et al., Photoacoustic image-guided biomimetic nanoparticles targeting rheumatoid arthritis, *Proc. Natl. Acad. Sci. USA* 119 (43) (2022), e2213373119.
- [47] C. Zhao, et al., Multimodal VEGF-targeted contrast-enhanced ultrasound and photoacoustic imaging of rats with inflammatory arthritis: using dye-VEGF-antibody-loaded microbubbles, *Ultrasound Med. Biol.* 46 (9) (2020) 2400–2411.
- [48] C. Zhao, et al., Multimodal photoacoustic/ultrasonic imaging system: a promising imaging method for the evaluation of disease activity in rheumatoid arthritis, *Eur. Radiol.* 31 (2021) 3542–3552.
- [49] M. Yang, et al., Synovial oxygenation at photoacoustic imaging to assess rheumatoid arthritis disease activity, *Radiology* 306 (1) (2023) 220–228.
- [50] C. Zhao, et al., The potential of photoacoustic techniques in inflammatory arthritis: what can it do to assist conventional imaging methods? *Chin. J. Acad. Radiol.* 4 (2) (2021) 79–87.
- [51] E.F. Rosloniec, K. Whittington, A. Proslovsky, D.D. Brand, Collagen-induced arthritis mouse model, *Curr. Protoc.* 1 (12) (2021), e313.
- [52] D.D. Brand, K.A. Latham, E.F. Rosloniec, Collagen-induced arthritis, *Nat. Protoc.* 2 (5) (2007) 1269–1275.
- [53] S. Alivernini, et al., Distinct synovial tissue macrophage subsets regulate inflammation and remission in rheumatoid arthritis, *Nat. Med.* 26 (8) (2020) 1295–1306.
- [54] C. Orr, et al., Synovial tissue research: a state-of-the-art review, *Nat. Rev. Rheumatol.* 13 (8) (2017) 463–475.
- [55] H.A. Elshabrawy, et al., The pathogenic role of angiogenesis in rheumatoid arthritis, *Angiogenesis* 18 (4) (2015) 433–448.

Zhen Wang is a master's student at the First Affiliated Hospital of Shantou University Medical College. His research interests are focused on small animal multimodal imaging and clinical translation.

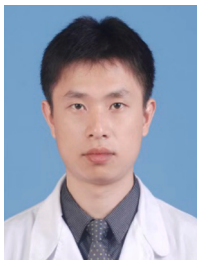




Zhuangzhuang Tong is a master's student at the Institute of Biophotonics, South China Normal University. His research interests are focused on photoacoustic/ultrasonic microscopy systems and physical algorithm design.



Erqi Wang is a master's student in the Institute of Biophotonics at South China Normal University. His research interests are focused on medical image processing.



Hongjiang Chen is an orthopedic surgeon at the First Affiliated Hospital of Shantou University Medical College. His research interests focus on ligament reconstruction and tendon bone healing, anti-osteoporosis, and the treatment of bone and soft tissue tumors.



Bo Yuan is a master's student at the Institute of Biophotonics, South China Normal University, has research interests in photoacoustics and ultrasound transducer development.



Guangshuai Nie is a master's student at the First Affiliated Hospital of Shantou University School of Medicine. His research interests are focused on the mechanism of exosomes in intervertebral disc lesions.



Zhiyang Wang is a postdoctoral fellow at the Institute of Biophotonics, South China Normal University. His research interests are focused on photoacoustic microscopy and its clinical applications.



Jia Hu is a master's student at the First Affiliated Hospital of Shantou University Medical College. His research interests are focused on the diagnosis and treatment of novel multifunctional bioprobe in arthritis.



Jun Hu is a professor of orthopedics at the First Affiliated Hospital of Shantou University Medical College. His research interests focus on bone and joint degeneration, anti-osteoporosis, and the treatment of bone and soft tissue tumors.



Weiyang Liu is an orthopedic surgeon at the First Affiliated Hospital of Shantou University Medical College. His research interests focus on ligament reconstruction and tendon bone healing, anti-osteoporosis, and the treatment of bone and soft tissue tumors.